Available online at www.sciencedirect.com
ScienceDirect
Journal of the European Ceramic Society 30 (2010) 759–767
www.elsevier.com/locate/jeurceramsoc

Processing and mechanical properties of Si_3N_4 composites employing polymer-derived SiAlOC as sintering aid

T. Plachký [a], Z. Lenčéš [a,*], Ľ. Hric [a], P. Šajgalík [a], P. Baláž [b], R. Riedel [c], H.-J. Kleebe [d]

[a] *Institute of Inorganic Chemistry, Slovak Academy of Sciences, Dúbravská cesta 9, SK-84536 Bratislava, Slovakia*
[b] *Institute of Geotechnics, Slovak Academy of Sciences, Watsonova 45, SK-04353 Košice, Slovakia*
[c] *Institut für Materialwissenschaft, Fachbereich Material- und Geowissenschaften, Technische Universität Darmstadt, Petersenstraße 23, 64287 Darmstadt, Germany*
[d] *Institut für Angewandte Geowissenschaften, Fachbereich Material- und Geowissenschaften, Technische Universität Darmstadt, Schnittspahnstr. 9, D-64287 Darmstadt, Germany*

Received 14 March 2009; received in revised form 6 August 2009; accepted 13 August 2009
Available online 1 October 2009

Abstract

Silicon nitride ceramics have been densified with polymer-derived SiAlOC sintering aid. Dense samples were prepared at relatively mild temperatures (1600 °C) from blends with 30 wt.% of pyrolysed SiAlOC additives. Decreasing the SiAlOC aid content to 15 wt.% resulted in porous Si_3N_4 samples (~85% rel. density). The properties of dense samples were influenced by the remaining SiAlOC glass (HV = 15.5 GPa, K_{IC} = 4 MPa $m^{1/2}$). Increasing the sintering temperature to 1780 °C for 5 min significantly changed the phase composition and properties of the composites. The major phase was O′-sialon in the sintered samples. Additional annealing of the samples at 1530 °C for 16 h further decreased the amount of the residual glassy phase and consequently affected the mechanical properties. The Vickers hardness of dense samples was 18.5 GPa and the fracture resistance ranged between 4.0 and 4.5 MPa $m^{1/2}$. The compressive creep test (1400 °C/100 MPa/24 h) of the SNA30-A sample sintered at 1600 °C for 30 min without an additional crystallisation step showed a promising low creep rate of 8.6×10^{-8} s^{-1}. Further improvement of creep resistance is expected for the crystallised samples.

Keywords: Precursor-organic; Composites; Creep; Spectroscopy; Oxynitrides

1. Introduction

Conversion of polysilazanes, polycarbosilazanes and polysiloxanes to dense ceramic fibres and foams has been intensively studied in the last decades.[1–4] However, the preparation of dense bulk ceramics from polymer-derived precursors is still a matter of research owing to the attractive shaping properties and low fabrication temperatures.[5] Amorphous bulk polymer-derived ceramics (PDCs) with interesting mechanical properties were prepared by warm pressing.[6,7] Preparation of a bulk crystalline body from polymer precursor, even with high ceramic yield of 85%, is still a problem because the polymer-to-ceramic conversion and the crystallisation of amorphous PDCs is accompanied by intrinsic shrinkage, serious cracking and pore formation. For that reason, crystalline reactive fillers were often used for the preparation of bulk PDCs.[4,8]

Among organosilicon polymers recently the polysiloxanes have been more intensively studied from the wide range of silicon-based polymer ceramic precursors because they can be handled in air, contrary to the oxygen and humidity sensitive polysilazanes.[9–12] Silicon oxycarbide (SiOC) is produced from polysiloxanes by crosslinking and pyrolysis. The incorporation of carbon into silicate glasses strengthens the molecular structure of the glass network, and thereby, improves the thermal and mechanical properties of SiOC glass.[3] By further heat-treatment, complex nanostructures are formed by phase separation in SiOC glass, in which nanocrystalline SiC, free carbon and remaining amorphous SiOC coexist.[14–17] These materials have exceptional properties, such as low creep rate and high thermal stability. Especially the excess free carbon phase plays an important role in the stability of amorphous and nanocrystalline phases.[13,18–20]

* Corresponding author. Tel.: +421 2 59410408; fax: +421 2 59410444.
E-mail address: Zoltan.Lences@savba.sk (Z. Lenčéš).

0955-2219/$ – see front matter © 2009 Elsevier Ltd. All rights reserved.
doi:10.1016/j.jeurceramsoc.2009.08.014

Table 1
Starting composition of samples and used sintering conditions.

Sample	Composition		Heating rate (°C/min)	Sintering conditions				
	Si_3N_4 (wt.%)	SiAlOC (wt.%)		Dwell at				Cooling rate (°C/min)
				1400 °C (min)	1600 °C (min)	1780 °C (min)	1530 °C (min)	
SNA30-A	70	30	20	30	30	–	–	30
SNA30-C	70	30	20	30	30	5	–	30
SNA30-D	70	30	20	30	30	5	960	30
SNA15	85	15	20	30	30	5	–	30

The basic silicon oxycarbide matrix can be doped by different elements, e.g. Al, Zr or Hf, having high affinity to oxygen or carbon, and improve the properties of SiOC.[3,21–23] Depending on the dopant composition and its volume fraction, the properties of SiOC can be varied in a rather wide range.

There are several reports on application of PDCs as a binder for crystalline ceramic powders.[24–27] However, this work is focused on the preparation of dense Si_3N_4/SiAlOC composites, where polymer-derived SiAlOC serves as a sintering aid. In comparison to Si_3N_4 materials densified with common crystalline oxide additives (Al_2O_3, MgO, CaO, RE_2O_3, etc.) at temperatures 1750–1800 °C for 1–2 h, the expected advantage of applying amorphous PDCs as sintering aid is the lower sintering temperature ($t_s < 1650$ °C) and shorter holding time ($\tau < 40$ min). For that reason the main goal of this work is to fabricate Si_3N_4/SiAlOC-based ceramics with high density at temperatures below 1650 °C and with mechanical properties comparable to conventionally prepared alumina containing Si_3N_4 ceramics at higher temperatures. Due to the expected partial decomposition and/or crystallisation of the SiAlOC phase above 1500 °C, thermodynamic analysis of the studied system was carried out together with dilatometric measurements prior to the sintering experiments. The microstructure, phase composition and some room temperature mechanical properties (HV, K_{IC}) of dense Si_3N_4/SiAlOC samples were evaluated. First results on the compressive creep resistance of the ceramic composite sintered at 1600 °C under 100 MPa load are also reported.

2. Experimental procedure

A commercial α-Si_3N_4 (SN-E10, Ube Industries, Japan) and in-lab prepared polymer-derived SiAlOC precursors (TU Darmstadt, Germany) have been used for the preparation of the starting mixtures. The SiAlOC precursor was synthesized by sol–gel method from poly-methylsilsesquioxane (MK polymer, Wacker-Bensil GmbH; Burghausen, Germany) with 23.6 wt.% of alumatrane (ABCR GmbH, Germany) in isopropanol solvent. The mixture was crosslinked and pyrolysed in a quartz tube up to 1100 °C in argon atmosphere for 2 h. The detailed process for the preparation of amorphous SiAlOC used in this work is described by Harshe et al.[28] The final composition of the pyrolysed polymer-derived sintering aid was $Si_{1.00}Al_{0.11}O_{1.90}C_{0.49}$. According to this composition, the crystalline product composed of SiC, SiO_2 and Al_2O_3 should contain 6.4 wt.% free carbon.

The Si_3N_4 matrix powder and pyrolysed SiAlOC additives were mixed in weight ratios 85:15 (samples SNA15) and 70:30 (samples SNA30). The mixtures were mechanically activated by high energy milling (Pulverisette 6, Fritsch, Germany) for 90 min in argon atmosphere. The starting powder mixtures passed through a 42 μm sieve were pressed into disks of 12 mm diameter with a uniaxial pressure of 100 MPa. The samples were densified by hot-pressing under a load of 30 MPa in static $N_2 + CO$ atmosphere. BN powder bed was used to minimize the possible reaction with the graphite die at elevated temperatures. The sample compositions and applied sintering conditions are listed in Table 1.

Densities of sintered samples were measured by the Archimedes method in mercury. Samples were cut, polished and etched in $CF_4 + O_2$ gas mixture (Plasma barrel etcher, Polaron PT7150). The microstructures of etched cross-sections of the hot-pressed samples were examined by SEM (Zeiss EVO 40 HV). Phase composition was identified by X-ray diffraction analysis (Bruker D8-Discover, Cu Kα radiation). Precise powder XRD measurements were conducted also in Debye-Scherrer transmission geometry (STOE Stadi-P, Germany) using Co Kα radiation ($\lambda = 0.178892$ nm); data acquisition was performed with a position-sensitive detector. The Vickers hardness (HV) was measured on polished cross-sections of pellets with a load of 9.8 N (LECO Vickers Hardness Tester, LV100). The indentation fracture resistance (K_{IC}) was measured on the same equipment with a load of 98 N and calculated according to Shetty's equation.[29] The presence and form of free carbon was investigated by Raman spectroscopy (Raman Spectrometer LabRam HR 800) using Ar-ion laser with $\lambda = 514.5$ nm. The compressive creep tests were carried out at 1400 °C in air under a load of 100 MPa for 24 h. Preliminary transmission electron microscopy (TEM) results were obtained with a FEI CM20 microscope operating at 200 keV.

3. Results and discussion

3.1. Thermodynamic analysis

The preliminary sintering curves recorded up to 1800 °C in nitrogen atmosphere showed that the softening of pyrolysed SiAlOC in Si_3N_4 matrix starts at ~1250 °C in SNA30 samples, followed by densification above 1320 °C. However, the densification rate was slow. A simple increase of sintering tem-

perature to accelerate the densification rate could not be applied in this case because partial decomposition of the polymer-derived SiAlOC sintering aid was observed above 1400 °C. For that reason thermodynamic analysis of the studied system was necessary. Only the proposed crystalline phases were taken into account in the calculations, because there are no available data for SiAlOC glasses.

Harshe et al.[28] reported that the phase separation in SiOC glass prepared from the same MK precursor (polymethylsilsesquioxane, Wacker-Besil PMS) used in this work starts at temperatures around 1300 °C and can be described by the following reaction:

$$SiO_xC_y(s) \rightarrow \beta\text{-}SiC(s) + SiO_2(a) + C(s) \quad (1)$$

The phase separation products are nanocrystalline β-SiC, amorphous silica and free carbon. Other authors showed that the devitrification of SiOC glass with different composition can start at temperatures even as low as 1200 °C.[30–33] However, the pyrolysed SiAlOC used in this work remains amorphous up to 1500 °C.[28] The presence of aluminium in the SiOC glass, together with free carbon inhibits crystobalite formation and devitrification of the amorphous SiAlOC matrix. Owing to this property, the densification of Si_3N_4 with SiAlOC additive should be easier compared to more rigid SiOC aid.[34] However, above 1500 °C the decomposition of SiAlOC can retard the densification of Si_3N_4 due to gas formation. Our preliminary results showed mass loss in SNA30 samples above 1430 °C in nitrogen atmosphere. At these temperatures, in addition to the crystallisation of β-SiC from amorphous SiAlOC, carbothermal reduction of silica can proceed according to the overall reaction (2), which includes reactions (3) and (4) with SiO(g) as an intermediate product/reactant. It was reported that all SiC(s), Si_3N_4(s) and Si_2N_2O(s) formation from SiO_2 occurs via the reaction with gaseous SiO(g).[35] Although the equilibrium rate constant K_p is low for reaction (2), at these temperatures only SiO_2 nanodomains are present in the system studied herein and their reactivity with excess free graphene is expected to be much higher as compared to the micrometer size crystalline grains the JANAF data are based on:

$$SiO_2(s) + 3C(s) \rightarrow SiC(s) + 2CO(g)$$
$$K_p(1430\,^\circ C) = 0.072 \quad (2)$$

$$SiO_2(s) + C(s) \rightarrow SiO(g) + CO(g) \quad (3)$$

$$SiO(g) + 2C(s) \rightarrow SiC(s) + CO(g) \quad (4)$$

Contrary to the desirable formation of SiC via reaction (2), silica reacts with SiC at higher temperatures and both can decompose into gaseous SiO and CO according to reaction (5):[36]

$$2SiO_2(s) + SiC(s) \rightarrow 3SiO(g) + CO(g) \quad (5)$$

Fig. 1 shows the equilibria curves obtained from the JANAF thermodynamic data[37] for both reactions (2) and (5). The CO pressure was kept between the two calculated equilibrium curves during sintering and annealing of samples, in order to promote the formation of SiC within the composite materials, while its

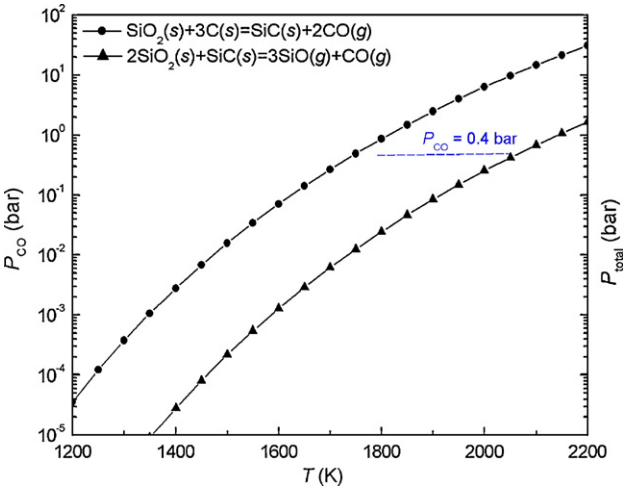

Fig. 1. Calculated equilibrium pressures of CO(g) and SiO(g) for the reactions (2) and (5).[15,37] Dashed line shows the applied CO(g) pressure.

decomposition by reaction (5) should be avoided. It is worth to point out that the lower bound in Fig. 1 represents the total equilibrium pressure of CO and SiO gaseous species of reaction (5).[15]

Apart from the CO pressure, particular attention must be paid to the partial pressure of nitrogen during sintering of Si_3N_4-based ceramics. The coexistence of Si_3N_4 matrix and SiC nanoparticles, which are formed from the SiAlOC glass at the applied hot-pressing temperatures $t \leq 1780$ °C, is limited by several factors: (*i*) decomposition of Si_3N_4 in inert atmosphere and/or low-pressure nitrogen ($p_{N2} < 0.1$ MPa) according to the reaction:

$$Si_3N_4(s) \rightarrow 3Si(l) + 2N_2(g), \quad (6)$$

and (*ii*) the nitridation of SiC in nitrogen atmosphere (reaction (7)), which can proceed at relatively low temperatures (~1440 °C and a nitrogen pressure 0.1 MPa[38]).

$$3SiC(s) + 2N_2(g) \rightarrow Si_3N_4(s) + 3C(s) \quad (7)$$

The equilibrium N_2 pressures for both reactions (6) and (7) were obtained from the JANAF thermodynamic tables.[37] Results of the thermodynamic calculations shown in Fig. 2 indicate the range of temperature and N_2 pressure, where SiC and Si_3N_4 coexist.

The thermodynamic considerations outlined above resulted in the application of a mixed N_2 and CO atmosphere during hot-pressing of Si_3N_4/SiAlOC pellets. Both CO and N_2 were introduced by gas-flow meters according to the required border conditions shown in Figs. 1 and 2.

With the exception of the main non-oxide components in the product, the oxygen containing crystalline phases have also to be considered, owing to the rather high amount of SiAlOC additive in the samples. At temperatures above 1400 °C, the amorphous SiAlOC glass can crystallise either by phase separation or by carbothermal reduction of amorphous silica in nitrogen atmosphere. Apart from SiC, SiO_2, Al_2O_3 and C, also Si_2N_2O can form.[40,41] Although the carbothermal reduction and nitridation of silica can result in Si_2N_2O formation according to the follow-

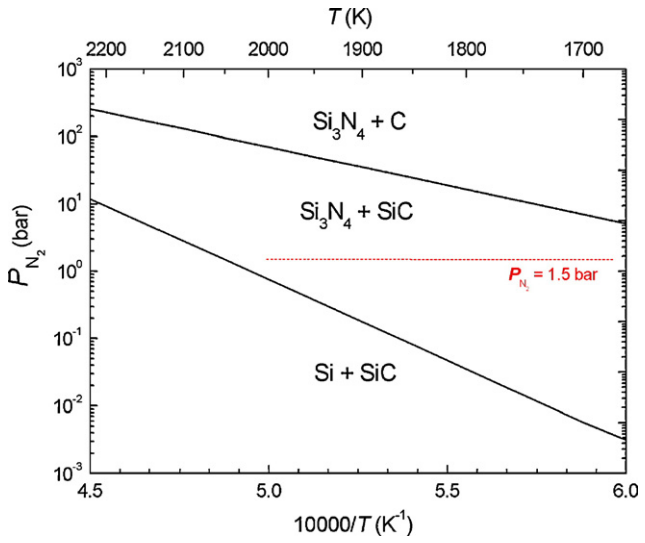

Fig. 2. Thermodynamic stability range for the coexistence of Si_3N_4 and SiC in nitrogen.[37,39] Dashed line shows the applied N_2 pressure.

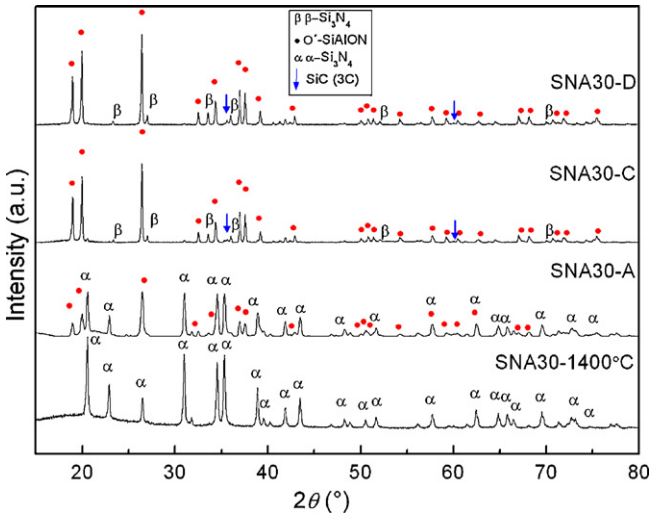

Fig. 3. XRD patterns of sintered SNA30 samples (see Table 1).

ing reaction:[42,43]

$$2SiO_2(s) + 3C(s) + N_2(g) \rightarrow Si_2N_2O(s) + 3CO(g),$$
$$\Delta G^\circ(1530\,^\circ C) = -64.6\,kJ\,mol^{-1}, \quad K_p = 75.1 \qquad (8)$$

the direct reaction between Si_3N_4 and silica cannot be avoided at the applied hot-pressing temperatures ($t \leq 1780\,^\circ C$):

$$1/2Si_3N_4(s) + 1/2SiO_2(s) \rightarrow Si_2N_2O(s),$$
$$\Delta G^\circ(1780\,^\circ C) = -92.4\,kJ\,mol^{-1}, \quad K = 226.8 \qquad (9)$$

Hence, the presence of Si_2N_2O in the sintered composites is expected.[44,45]

3.2. Sintering conditions and phase compositions

The temperature regime for the hot-pressing of Si_3N_4/SiAlOC samples was optimised for the samples with higher additive content (30 wt.%) on the base of previous thermodynamic calculations and recorded sintering curves up to 1800 °C. The first holding time was applied at 1400 °C for 30 min (Table 1) to promote densification via viscous flow. At this temperature, the viscosity of SiAlOC glass decreases ($t_g = 1250\,^\circ C$)[28] and the densification is initiated via viscous flow of the glassy phase. The second dwell at 1600 °C corresponds to the observed rapid densification rate at this temperature. An additional heating to 1780 °C for a short time (5 min) was applied in the case of sample SNA30-C to enhance nucleation of nanosized SiC from the SiAlOC glass.[43] After hot-pressing, a prolonged crystallisation of the SiAlOC glassy phase was carried out at 1530 °C for 16 h (sample SNA30-D, Table 1).

The densities of sintered samples are summarized in Table 2. Sample SNA30-A is almost fully dense after hot-pressing at 1600 °C for 30 min with a relatively high fraction of the amorphous phase (and a low fraction of nanosized pores), as confirmed by SEM analysis. The decreased densities of samples SNA30-C (97.8%) and *D* (96.7%) were due to the mass loss and pore formation caused by the partial decomposition of the residual SiAlOC glass. Although the mass loss of samples with 15 wt.% of SiAlOC was negligible, their densification was difficult and resulted in a relative density as low as 85%. The result indicates that 15 wt.% of pyrolysed SiAlOC sintering aid is not sufficient for densification of Si_3N_4 under the applied experimental conditions.

The X-ray diffraction patterns of hot-pressed SNA30 samples are compared in Fig. 3. The phase composition of sample sintered at 1400 °C for 30 min is only the original α-Si_3N_4 and the amorphous SiAlOC. This result together with TEM observation that the Si_3N_4 particles have sharp, not dissolved edges confirms that the main densification mechanism at this temperature is the viscous flow. The major crystalline phase in sample SNA30-A after hot-pressing at 1600 °C is α-Si_3N_4, but the formation of O′-sialon with very low aluminium substitution was observed. O′-sialon is a solid solution derived from silicon oxynitride (Si_2N_2O) by substitution of Al–O for Si–N and can be represented by the formula $Si_{2-x}Al_xO_{1+x}N_{2-x}$. The *x* value can vary from zero to 0.2.[46,47] The formation of O′-sialon confirms that

Table 2
Densities and phase composition of SNA samples.

Sample	Density (g cm^{-3})	Rel. density (%)	Phase composition
SNA30-A	2.87	99.8	α-Si_3N_4, O′-sialon, SiAlOC (amorph.)
SNA30-C	2.81	97.8	O′-sialon, β-Si_3N_4, SiC
SNA30-D	2.78	96.7	O′-sialon, β-Si_3N_4, SiC
SNA15	2.56	85.1	O′-sialon, β-Si_3N_4, SiC

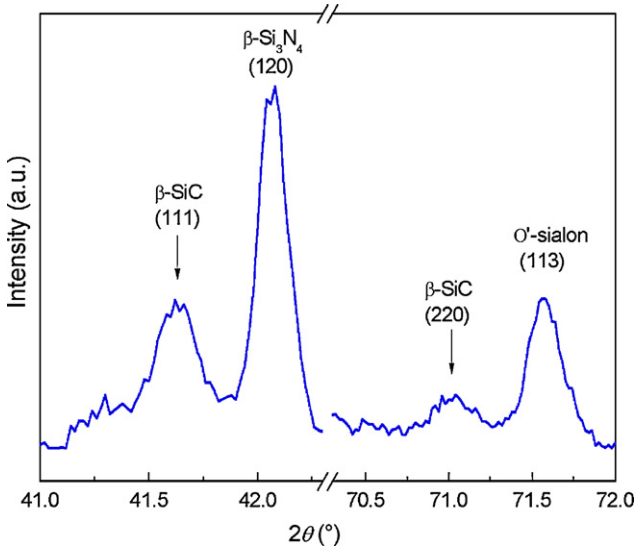

Fig. 4. Detailed XRD pattern of SNA30-D sample (Co Kα radiation) confirming the presence of (nano)crystalline β-SiC.

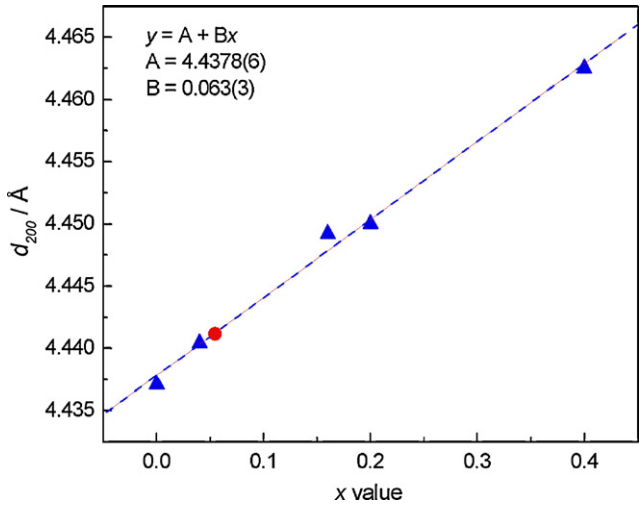

Fig. 5. Dependence of the (2 0 0) plane distance d of O′-sialon on x value in $Si_{2-x}Al_xO_{1+x}N_{2-x}$. Data for O′-sialon are from Refs. Lindquist et al.[50] and Trigg and Jack[46] and for pure Si_2N_2O ($x=0$) from Sjöberg et al.[51] (PDFs No. 33-1162, 79-1539 and 79-1540). The calculated Al substitution in sample SNA30-D with $d(2\,0\,0)=4.4410$ Å is $x=0.056$ (symbol ●).

at 1600 °C α-Si_3N_4 dissolves in the SiAlOC melt and the densification proceeds also via liquid phase sintering. Apart from the crystalline phases determined, a broad peak near 20° to 22° in the SNA30-A sample indicates the presence of the remaining amorphous silica and/or SiOC glass.[31]

The main crystalline phase was O′-sialon in samples SNA30-C and D. It was shown that O′-sialon preferably forms at lower temperatures (1500–1750) °C, while at ∼1800 °C O′-sialon redissolves and a more nitrogen-rich β′-sialon phase precipitates.[48,49] According to these observations, the conditions for O′-sialon formation were favourable in our experiments, suppressing the nucleation of β′-sialon. The presence of crystalline SiC was not confirmed by XRD analysis in sample SNA30-A. However, β-SiC diffraction peaks were observed in samples SNA30-C and D annealed at 1780 °C (Fig. 4) parallel to a high degree of α- to β-Si_3N_4 phase transformation even within 5 min. The shrinkage of samples during holding time at 1780 °C for 5 min was negligible. As it was mentioned above, the main purpose of the short annealing at 1780 °C was to enhance the crystallisation and partly the growth of SiC nanoparticles. The SiC particle size after 5 min holding time at 1780 °C was in the range 30–60 nm. These nanoparticles have a positive influence on the hardness, strength and creep resistance of O′-sialon matrix (see Section 3.5).

The aluminium content in O′-sialon ($Si_{2-x}Al_xO_{1+x}N_{2-x}$) of the SNA30-D sample was determined from the precise XRD measurements carried out on a STOE diffractometer operated in transmission mode. It is known that the orthorhombic structure of Si_2N_2O ($x=0$ in O′-sialon) is composed of puckered Si–N layers linked by Si–O–Si bridges. Within the solid solubility range in $Si_{2-x}Al_xO_{1+x}N_{2-x}$, the unit-cell parameter a perpendicular to the Si–N planes increases with increasing aluminium and oxygen content, while no significant change is seen for the other unit-cell parameters.[46] Lindquist et al.[50] found a nearly linear correlation between the (Si,Al)–O(2) bond length and the x value in $Si_{2-x}Al_xO_{1+x}N_{2-x}$.

In this work, the substituted Al content in the oxynitride structure was determined from the shift of the (2 0 0) diffraction peak. The position of the (2 0 0) peak of O′-sialons ($Si_{2-x}Al_xO_{1+x}N_{2-x}$) with x values 0.04, 0.16 and 0.40 were taken from the work of Lindquist et al.[50], $x=0.2$ from Trigg and Jack (PDF No. 40-672),[46] and the data for pure Si_2N_2O were published by Sjöberg et al.[51] The dependence of the (2 0 0) peak position on the x value is shown in Fig. 5. Using the linear fit of the data in Fig. 5 and the plane distance $d(2\,0\,0)=4.4410$ Å from the diffraction pattern of SNA30-D specimen, the value of $x=0.056$ was calculated, which is consistent with the result of $x=0.06$ obtained by elemental analysis of this sample. The results suggest that this experimental procedure can be used for the rough estimation of the aluminium substitution in O′-sialon.

According to the starting composition of the amorphous SiAlOC sintering aid, free carbon should be present in the crystalline product. Although carbon was not apparent from the XRD and SEM investigations, preliminary TEM investigations showed the presence of turbostratic graphite (compare Fig. 7). Therefore, Raman spectroscopy studies were also carried out on all hot-pressed composites.

3.3. Raman spectroscopy

Disordered graphite-like carbon was confirmed by Raman spectroscopy in all SNA30 samples, as shown in Fig. 6. The spectra have characteristic bands observed in disordered sp^2 carbons: the disordered D band located at ∼1355 cm^{-1} and the "graphite-like" G band lying between 1500 and 1600 cm^{-1} (1581 ± 1 cm^{-1} for graphite[52,53]). The D peak originates from the breathing mode (A_{1g}) of aromatic rings and is active only in the disordered network of imperfect graphite structure. The G peak arises from the in-plane bond stretching (E_{2g}) of carbon atom pairs hybridized in sp^2 configuration.[54] Near the G band, the so-called D' band can also be seen in Fig. 6,

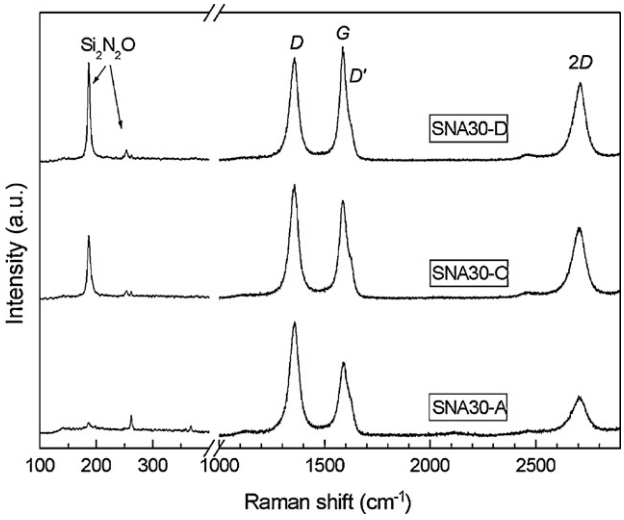

Fig. 6. Raman spectra of SNA30 samples show the presence of *D*, *G*, *D*′ and 2*D* carbon bands. Si_2N_2O peaks are present in samples sintered at 1780 °C for 5 min.

which was observed especially in defected graphite around 1620 cm^{-1}.[52]

Except for the first order Raman scattering also the second-order *D* peak appears at ~2700 cm^{-1}, referred to as 2*D* band (two phonon process).[55] The second-order peak arises in disordered graphite with a high *c*-axis ordering and, therefore, a partial clustering of carbon is assumed in the SNA30 samples. Due to this fact, we have tried to determine the in-plane cluster size L_a of carbon particles from the ratio of the *D* and *G* band intensities I_D/I_G. Tuinstra and Koenig[56] showed that the ratio I_D/I_G is inversely proportional to the diameter or length (L_a) of nanographite particles according to the following equation:

$$\frac{I_D}{I_G} = \frac{C(\lambda)}{L_a} \tag{10}$$

where $C = 4.4$ nm for $\lambda = 514.5$ nm. However, the minimum of L_a for which Eq. (10) was verified is 2 nm. Cançado et al.[57] derived a general expression for the calculation of L_a from the integrated intensity ratio I_D/I_G, which includes also the excitation laser energy (expressed here with the laser wavelength $\lambda = hc/E$), which has an influence on the line intensities:

$$L_a(nm) = (2.4 \times 10^{-10})\lambda^4 \left(\frac{I_D}{I_G}\right)^{-1} \tag{11}$$

where λ is the laser line wavelength in nanometer units.

The results of Raman spectroscopy with the position of *D* and *G* bands and the calculated in-plane crystal size of graphite L_a are summarized in Table 3. The expression for the L_a calculation based on Tuinstra and Koenig[56] (L_{a1}) is more applicable to nanocrystalline graphite since it underestimates the L_a[20,32] monitored in the SNA30 samples. More reliable values of L_a for the mixed amorphous-crystalline materials studied in this work gives the general equation of Cançado et al.[57] (L_{a2} in Table 3). The calculated crystal size of graphitic carbon is in the range of 9–16 nm in the SNA30 samples, where L_a increases with rising temperature and annealing time. Preliminary TEM observations

Table 3
Position of *D* and *G* bands of carbon in Raman spectra and the calculated in-plane crystal size L_a of graphite using eqv. from Refs. Tuinstra and Koenig[56] and Cançado et al.[57].

Sample	*D* band (cm^{-1})	*G* band (cm^{-1})	I_D/I_G	L_{a1}[56] (nm)	L_{a2}[57] (nm)
SNA30-A	1358	1589	1.819	1.82	9.25
SNA30-C	1358	1588	1.135	1.44	14.82
SNA30-D	1358	1587	1.033	1.37	16.28

are in good agreement with the calculated size of L_a since they reveal features of turbostratic graphite ranging between 10 and 20 nm (Fig. 7).

3.4. Microstructure

The microstructures of sintered SNA30-A, SNA30-C and the annealed SNA30-D samples are shown in Fig. 8. Sample SNA30-A consists of equiaxed α-Si_3N_4 grains with a particle diameter of about 0.3 μm embedded in the O′-sialon matrix. The α-Si_3N_4 grains can be distinguished from the sialon phase owing to their different etching rate in CF_4 and O_2 mixture, α-Si_3N_4 is etched faster (equiaxed pits in Fig. 8a). Few islands of the residual SiAlOC glass are dispersed throughout the entire bulk of the samples.

The microstructures of samples SNA30-C and D are composed of elongated O′-sialon grains with a diameter of (0.2–0.4) μm and a length up to 1.5 μm. Fig. 8b and c confirm that the temperature of crystallisation was set low enough to avoid abnormal growth of O′-sialon grains. β-SiC nanoparticles with a diameter up to 50 nm are located mainly intergranularly between O′-sialon grains. These are formed mainly by phase separation of SiAlOC, however the carbothermal reduction of the SiAlOC glass via reaction (2) cannot be excluded. Few nanosized pores can be found in both SNA30-C and SNA30-D samples as a result of reactions (1)–(5), i.e., oxycarbide glass decomposition, which proceed at the employed sintering tem-

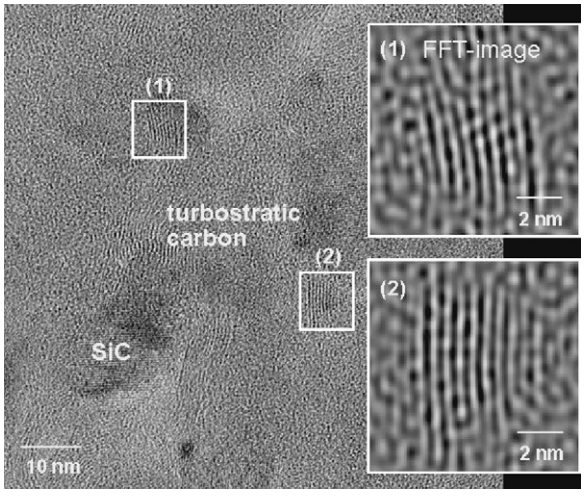

Fig. 7. HRTEM image of a grain-boundary region within sample SNA30 revealing the formation of turbostratic carbon in close proximity to SiC nanoparticles. Note that the size of the excess free carbon phase of approximately 10 nm (cf. Fourier-filtered images to the right) is in good agreement with the Raman data.

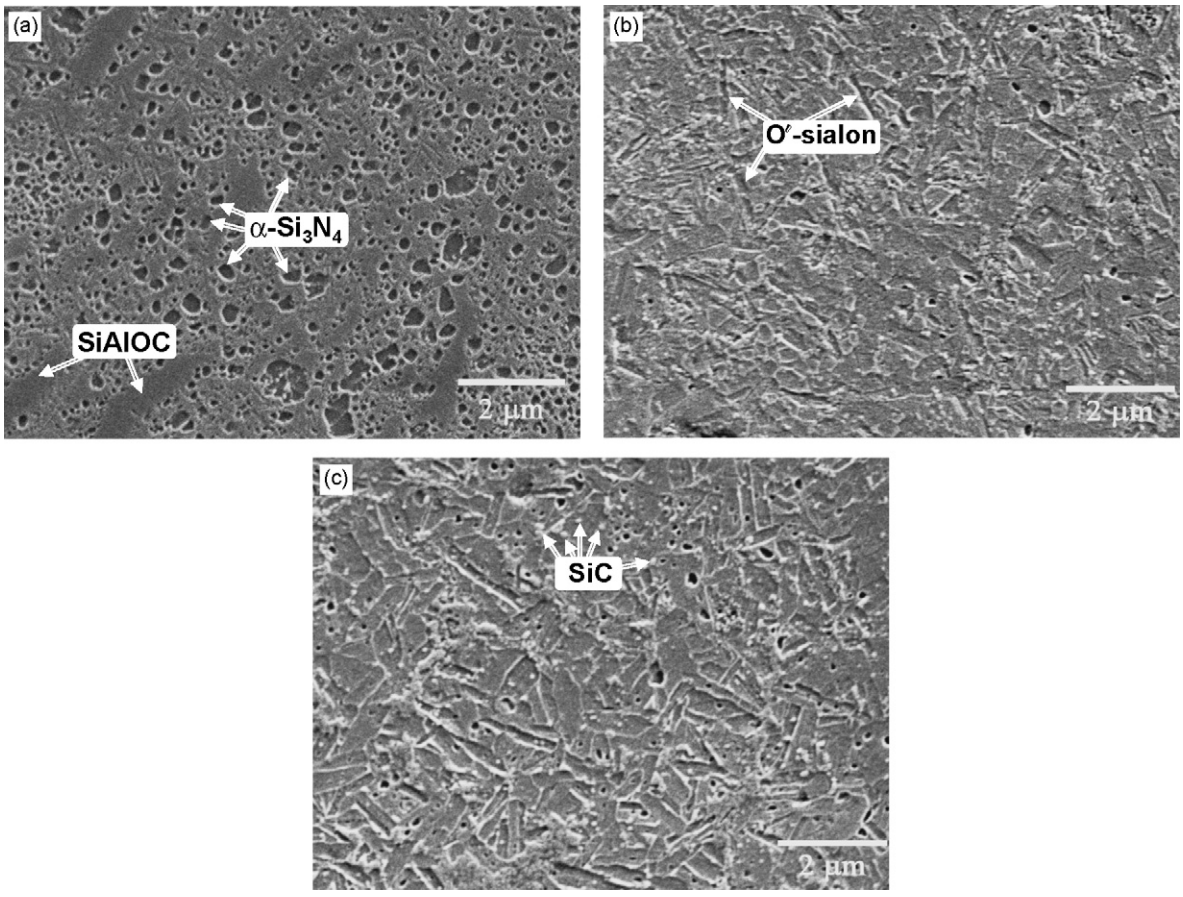

Fig. 8. SEM micrographs of sintered SNA30 samples: (a) SNA30-A: 1600 °C/30 min, (b) SNA30-C: 1780 °C/5 min and (c) SNA30-D: 1780 °C/5 min and crystallisation at 1530 °C/16 h. Etched out pits are α-Si_3N_4, needle-like grains are O′-sialons.

peratures $t_s \leq 1780$ °C. The authors are confident that these pores can be eliminated by further optimising the corresponding temperature and gas regimes.

3.5. Mechanical properties and creep resistance

Room temperature mechanical properties of the sintered SNA30 samples are summarized in Fig. 9. The lower hardness of sample SNA30-A is caused by the higher amount of residual SiAlOC glass, which has a hardness of approximately 3–5 GPa.[28] The highest hardness and indentation fracture resistance was observed for sample SNA30-C after sintering at 1780 °C for 5 min ($HV = 18.6$ GPa, $K_{IC} = 4.5$ MPa $m^{1/2}$). The results correspond with the published mechanical properties of Si_3N_4/Si_2N_2O composites prepared by conventional sintering at higher temperatures and longer holding times.[58–60] It is known that the hardness of commercial hot-pressed β-Si_3N_4 ceramics is 16 GPa and the hardness values for O′-sialon and Si_2N_2O materials vary from 17 to 20 GPa, depending on the preparation route and the sintering additives used.[61,62] Moreover, the SiC nanoparticles have also a positive influence on the mechanical properties of silicon oxynitride-based matrix.[63] The hardness and fracture resistance of sample SNA30-D slightly decreased, as compared to sample SNA30-C, owing to the higher porosity (3–5%) that formed during crystallisation. Despite the promising mechanical properties, the crystallisation conditions require further optimisation.

The first compressive creep tests of SNA30-A sample (without the crystallisation step) at 1400 °C and a load of 100 MPa showed a promising low creep rate of 8.6×10^{-8} s^{-1}, which is lower than the compressive creep rate of a comparable alumina-containing Si_3N_4 sample with 5% Y_2O_3 and 2%

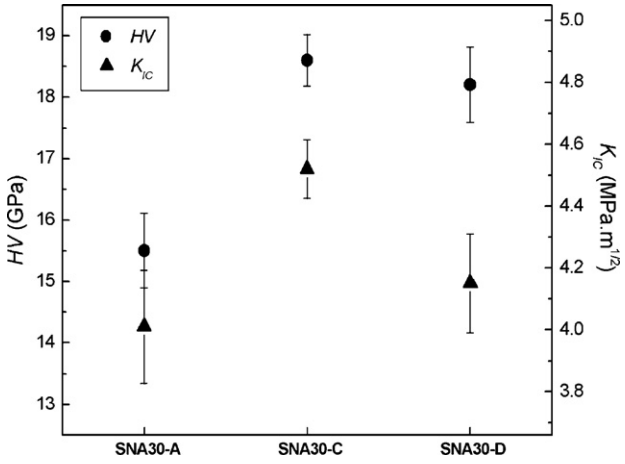

Fig. 9. Vickers hardness (HV) and indentation fracture resistance (K_{IC}) of SNA30 samples.

Al_2O_3 additives.[64] Further improvement of the creep resistance of Si_3N_4/SiAlOC ceramic composite is expected upon optimised/tailored crystallisation.

4. Conclusions

Crystalline oxide sintering additives commonly used for the densification of Si_3N_4 ceramics, have been replaced by an amorphous polymer-derived SiAlOC sintering aid. Samples with a relative density of 98–99% were prepared by hot-pressing at 1600 °C for 30 min from blends with 30 wt.% SiAlOC additive. The resulting mechanical properties of the samples are strongly affected by the volume fraction of the remaining SiAlOC glass. An additional short sintering at 1780 °C for 5 min had a major influence on both phase composition and mechanical response of the samples. The predominant phase determined upon sintering was O′-sialon, which in turn governed the mechanical properties of the composite materials ($HV = 18.6$ GPa, $K_{IC} = 4.5$ MPa $m^{1/2}$). The substituted Al content in the O′-sialon structure ($Si_{2-x}Al_xO_{1+x}N_{2-x}$) was determined from the shift of the (2 0 0) diffraction peak and is $x = 0.056$, which is consistent with the value of $x = 0.06$ obtained from elemental analysis.

The presence of carbon was confirmed by Raman spectroscopy and the in-plane crystallite size of graphitic carbon was calculated from the Raman spectra to range from 9 to 16 nm, which is in good agreement with TEM observations.

The compressive creep test (1400 °C/100 MPa/24 h) of the dense SNA30-A sample sintered at 1600 °C for 30 min showed a rather promising low creep rate of 8.6×10^{-8} s^{-1}, which is expected to be further improved via a long-term annealing step, promoting the precipitation of nanosized SiC which in turn limits grain-boundary sliding.

Acknowledgements

This work was supported by the 6th FP EU project PolyCerNet and partly by the Slovak Grant Agencies APVV-13-06, APVV-0448-06 and VEGA Project No. 2/7171/27. R.R. acknowledges the financial support by the Fonds der Chemischen Industrie, Frankfurt, Germany, and P.B. the financial support by LPP-0196-06, Slovakia. The authors are grateful to Dr. F. Lofaj from the Institute of Materials Research, SAS, Slovakia for the compressive creep tests.

References

1. Wills, R. R., Markle, R. A. and Mukherjee, S. P., Siloxanes, silanes and silazanes in the preparation of ceramics and glasses. *J. Am. Ceram. Soc. Bull.*, 1983, **62**(8), 904–911.
2. Yajima, S., Special heat-resisting materials from organometallic polymers. *J. Am. Ceram. Soc. Bull.*, 1983, **62**(8), 893–898.
3. Riedel, R., Mera, G., Hauser, R. and Klonczynski, A., Silicon-based polymer-derived ceramics: synthesis, properties and applications—a review. *J. Ceram. Soc. Jpn.*, 2006, **114**(6), 425–444.
4. Greil, P., Active filler-controlled pyrolysis of preceramic polymers. *J. Am. Ceram. Soc.*, 1995, **78**(4), 835–848.
5. Rice, R. W., Ceramics from polymer pyrolysis, opportunities and needs—a materials perspective. *J. Am. Ceram. Soc. Bull.*, 1983, **62**(8), 889–892.
6. Seitz, J. and Bill, J., Production of compact polysilazane-derived Si/C/N ceramics by plastic forming. *J. Mater. Sci. Lett.*, 1996, **15**, 391–393.
7. Konetschny, C., Galusek, D., Reschke, S., Fasel, C. and Riedel, R., Dense silicon carbonitride ceramics by pyrolysis of cross-linked and warm pressed polysilazane powders. *J. Eur. Ceram. Soc.*, 1999, **19**, 2789–2796.
8. Seyferth, D., Bryson, N., Workman, D. P. and Sobon, C. A., Preceramic polymers as "reagents" in the preparation of ceramics. *J. Am. Ceram. Soc.*, 1991, **74**(10), 2687–2689.
9. Zhang, H. and Pantano, C., Synthesis and characterization of silicon oxycarbide glasses. *J. Am. Ceram. Soc.*, 1990, **73**(4), 958–963.
10. Renlund, G. M. and Prochazka, S., Silicon oxycarbide glasses. Part I. Preparation and chemistry. *Mater. Res.*, 1991, **6**(12), 2716–2722.
11. Babonneau, F., Sorarù, G. D., D'Andrea, G., Dire, S. and Bois, L., Silicon oxycarbide glasses from sol–gel precursors. *Mater. Res. Soc. Symp. Proc.*, 1992, **271**, 789–794.
12. Sorarù, G. D., Silicon oxycarbide glasses from gels. *J. Sol–Gel Sci. Technol.*, 1994, **2**, 843–848.
13. Riedel, R., Ruswisch, L. M., An, L. and Raj, R., Amorphous silicoboron carbonitride ceramic with very high viscosity at temperatures above 1500 °C. *J. Am. Ceram. Soc.*, 1998, **81**, 3341–3344.
14. Monthioux, M. and Delverdier, O., Thermal behaviour of (organosilicon) polymer-derived ceramics. V. Main facts and trends. *J. Eur. Ceram. Soc.*, 1996, **16**, 721–737.
15. Saha, A. and Raj, R., Crystallization maps for SiOC amorphous ceramics. *J. Am. Ceram. Soc.*, 2007, **90**(2), 578–583.
16. Kleebe, H.-J., Turquat, C. and Sorarù, G. D., Phase separation in an SiCO glass studied by transmission electron microscopy and electron energy-loss spectroscopy. *J. Am. Ceram. Soc.*, 2001, **84**(5), 1073–1080.
17. Esfehanian, M., Oberacker, R., Fett, T. and Hoffmann, M. J., Development of dense filler-free polymer-derived SiOC ceramics by field-assisted sintering. *J. Am. Ceram. Soc.*, 2008, **91**(11), 3803–3805.
18. Kleebe, H.-J., Turquat, C. and Sorarù, G. D., Phase separation in a SiCO glass studied by transmission electron microscopy and electron energy-loss spectroscopy. *J. Am. Ceram. Soc.*, 2001, **84**(5), 1073–1080.
19. Kleebe, H.-J. and Blum, Y., SiOC ceramics with high excess free carbon. *J. Eur. Ceram. Soc.*, 2008, **28**(5), 1037–1042.
20. Kleebe, H.-J., Gregori, G., Babonneau, F., Blum, Y. D., MacQueen, D. B. and Masse, S., Evolution of C-rich SiOC ceramics. Part-I. Characterization by integral spectroscopic techniques: solid-state NMR and Raman spectroscopy. *Int. J. Mater. Res.*, 2006, **97**(6), 699–709.
21. Babonneau, F., Sorarù, G. D., Thorne, K. J. and Mackenzie, J. D., Chemical characterization of Si–Al–O–C precursor and its pyrolysis. *J. Am. Ceram. Soc.*, 1991, **74**(7), 1725–1728.
22. Brahmandam, S. and Raj, R., Novel composites constituted from hafnia and a polymer-derived ceramic as an interface: phase for severe ultrahigh temperature applications. *J. Am. Ceram. Soc.*, 2007, **90**(10), 3171–3176.
23. Ionescu, E., Linck, C., Papendorf, B. and Riedel, R., Synthesis and characterisation of novel polymer-derived ZrO_2/SiOC and HfO_2/SiOC-based ceramic nanocomposites. In *In Book of Abstracts of the 8th Conference on Solid State Chemistry*, 2008, ISBN 978-80-224-1019-9, p. 84.
24. Riedel, R., Seher, M., Mayer, J. and Vinga Szabó, D., Polymer-derived Si-based bulk ceramics. Part I. Preparation, processing and properties. *J. Eur. Ceram. Soc.*, 1995, **15**, 703–715.
25. Dressler, W., Greiner, A., Seher, M. and Riedel, R., Fabrication of nanostructured ceramics by hybrid processing. *Nanostruct. Mater.*, 1995, **6**, 481–484.
26. Kleebe, H.-J., Schmidt, H., Lehner, W. and Ziegler, G., Organometallic precursors, an alternative route for the doping of silicon nitride powders? *J. Eur. Ceram. Soc.*, 2002, **22**, 955–961.
27. Bernardo, E., Colombo, P. and Hampshire, S., SiAlON-based ceramics from filled preceramic polymers. *J. Am. Ceram. Soc.*, 2006, **89**(12), 3839–3842.
28. Harshe, R., Balan, C. and Riedel, R., Amorphous Si(Al)OC ceramic from polysiloxanes: bulk ceramic processing, crystallization behaviour and applications. *J. Eur. Ceram. Soc.*, 2004, **24**, 3471–3482.
29. Shetty, D. K., Wright, I. G., Mincer, P. N. and Clauer, A. H., Indentation fracture of WC-Co cermets. *J. Mater. Sci.*, 1985, **20**, 1873–1882.

30. Bréquel, H., Parmentier, J., Walter, S., Badheka, R., Trimmel, G., Masse, S., Latournerie, J., Dempsey, P., Turquat, C., Desmartin-Chomel, A., Le Neindre-Prum, L., Jayasooriya, U. A., Hourlier, D., Kleebe, H.-J., Sorarù, G. D., Enzo, S. and Babonneau, F., Systematic structural characterisation of the high temperature behavior of nearly-stoichiometric silicon oxycarbide glasses. *Chem. Mater.*, 2004, **16**(13), 2585–2598.
31. Sorarù, G. D., Modena, S., Guadagnino, E., Colombo, P., Egan, J. and Pantano, C., Chemical durability of oxycarbide glasses. *J. Am. Ceram. Soc.*, 2002, **85**(6), 1529–1536.
32. Gregori, G., Kleebe, H.-J., Blum, Y. D. and Babonneau, F., Evolution of C-rich SiOC ceramics. Part-II. Characterization by high lateral resolution techniques: electron energy-loss spectroscopy, high-resolution TEM and energy-filtered TEM. *Int. J. Mater. Res.*, 2006, **97**(6), 710–720.
33. Gregori, G., Kleebe, H.-J., Readey, D. W. and Sorarù, G. D., Energy-filtered TEM study of Ostwald ripening of Si nanocrystals in SiCO glasses. *J. Am. Ceram. Soc.*, 2006, **89**(5), 1699–1703.
34. Hric, L., Preparation of SiC-based ceramics with uncommon SiOC sintering aids. *PhD thesis*, Slovak Technical University, Bratislava, Slovakia, 2008.
35. Wada, H., Wang, M.-J. and Tien, T.-Y., Stability of phases in the Si–C–N–O system. *J. Am. Ceram. Soc.*, 1988, **71**(10), 837–840.
36. Filsinger, D. H. and Bourrie, D. B., Silica to silicon: key carbothermic reactions and kinetics. *J. Am. Ceram. Soc.*, 1990, **73**(6), 1726–1732.
37. Chase Jr., M. W., NIST-JANAF thermochemical tables, fourth edition (Part I and Part II). *J. Phys. Chem. Ref., Monograph 9*, 1998.
38. Nickel, K. G., Hoffmann, M. J., Greil, P. and Petzow, G., Thermodynamic calculations for the formation of SiC-Whisker-reinforced Si_3N_4 ceramics. *Adv. Ceram. Mater.*, 1988, **3**, 557–562.
39. Herrmann, M., Schubert, C., Rendtel, A. and Hübner, H., Silicon nitride/silicon carbide nanocomposite materials. I. Fabrication and mechanical properties at room temperature. *J. Am. Ceram. Soc.*, 1998, **81**(5), 1095–1108.
40. Durham, S. J. P., Shanker, K. and Drew, R. A. L., Thermochemistry of the Si–O–C–N system with relation to the formation of silicon nitride. *Can. Metall. Quart.*, 1991, **30**, 39–43.
41. Kleebe, H.-J., Braue, W., Schmidt, H., Pezzotti, G. and Ziegler, G., Transmission electron microscopy of microstructures in ceramic materials. *J. Eur. Ceram. Soc.*, 1996, **16**(3), 339–351.
42. Siddiqi, S. A. and Hendry, A., The microstructure of dense low-cost silicon oxynitride. In *Special Ceramics 8*, *vol. 37*, ed. S. P. Howlett and D. Taylor. Proc. Br. Ceram. Soc., 1986, pp. 1–13.
43. Lenčéš, Z., Bellosi, A. and Monteverde, F., Factors influencing the crystallization and the densification of ultafine Si/N/C powders. *Mater. Chem. Phys.*, 1995, **41**, 46–54.
44. Yu, G.-E., Edirisinghe, M., Finch, D., Ralph, B. and Parrick, J., Synthesis of silicon oxynitride from a polymeric precursor. *J. Mater. Sci.*, 1995, **30**, 5371–5380.
45. Scheffler, M., Pippel, E., Woltersdorf, J. and Greil, P., In situ formation of SiC–Si_2ON_2 micro-composite materials from preceramic polymers. *Mater. Chem. Phys.*, 2003, **80**, 565–572.
46. Trigg, M. B. and Jack, K. H., Solubility of aluminium in silicon oxynitride. *J. Mater. Sci. Lett.*, 1987, **6**, 407–408.
47. Pezzotti, G., Kleebe, H.-J., Ota, K. and Yabuta, K., Suppression of viscous grain-boundary sliding in dilute SiAlON ceramic. *J. Am. Ceram. Soc.*, 1997, **80**(9), 2349–2354.
48. Sun, W. Y., Li, W. L., Yan, D. S. and Yen, T. S., Studies on the phase distribution in (O′+β′)-sialon composites. *J. Eur. Ceram. Soc.*, 1989, **5**, 99–104.
49. Duan, R.-G., Roebben, G., Vleugels, J. and Van der Biest, O., Optimization of microstructure and properties of in situ formed β–O′–sialon–TiN composite. *Mater. Sci. Eng. A*, 2006, **427**, 195–202.
50. Lindquist, O., Sjöberg, J., Hull, S. and Pompe, R., Structural changes in O′-sialons, $Si_{2-x}Al_xN_{2-x}O_{1+x}$, $0.04 \leq x \leq 0.40$. *Acta Cryst.*, 1991, **B47**, 672–678.
51. Sjöberg, J., Helgesson, G. and Idrestedt, I., Refinement of the structure of Si_2N_2O. *Acta Cryst.*, 1991, **C47**, 2438–2441.
52. Nemanich, R. J. and Solin, S. A., First- and second-order Raman scattering from finite-size crystals of graphite. *Phys. Rev. B*, 1979, **20**, 392–401.
53. Coleman, J. N., Dalton, A. B., Curran, S., Rubio, A., Davey, A. P., Drury, A., McCarthy, B. and Ferrari, A. C., Raman spectroscopy of graphene and graphite: disorder, electron–phonon coupling, doping and nonadiabatic effects. *Solid State Commun.*, 2007, **143**, 47–57.
54. Ferrari, A. C. and Robertson, J., Interpretation of Raman spectra of disordered and amorphous carbon. *Phys. Rev. B*, 2000, **61**(20), 14095–14107.
55. Faugeras, C., Nerrière, A., Potemski, M., Mahmood, A., Dujardin, E., Berger, C. and de Heer, W. A., Few-layer graphene on SiC, pyrolitic graphite, and graphene: a Raman scattering study. *Appl. Phys. Lett.*, 2008, **92**(1), 011914 (1–3).
56. Tuinstra, F. and Koenig, J. L., Raman spectrum of graphite. *J. Chem. Phys.*, 1970, **53**, 1126–1130.
57. Cançado, L. G., Takai, K., Enoki, T., Endo, M., Kim, Y. A., Mizusaki, H., Jorio, A., Coelho, L. N., Magalhães-Paniago, R. and Pimenta, M. A., General equation for the determination of the crystallite size L_a of nanographite by Raman spectroscopy. *Appl. Phys. Lett.*, 2006, **88**(16)., doi:10.1063/1.2196057, 163106 (1–3).
58. Lewis, M. H., Reed, C. J. and Butler, N. D., Pressureless-sintered ceramics based on the compound Si_2N_2O. *Mater. Sci. Eng.*, 1985, **71**, 87–94.
59. Billy, M., Boch, P., Dumazeau, C., Glandus, J. C. and Goursat, P., Preparation and properties of new silicon oxynitride based ceramics. *Ceram. Int.*, 1981, **7**(1), 13–18.
60. Ekström, T., Olsson, P.-O. and Holström, M., O′-sialon ceramics prepared by hot isostatic pressing. *J. Eur. Ceram. Soc.*, 1993, **12**, 165–176.
61. Larker, R., Reaction sintering and properties of silicon oxynitride densified by hot isostatic pressing. *J. Am. Ceram. Soc.*, 1992, **75**(1), 62–66.
62. Tong, Q., Wang, J., Li, Z. and Zhou, Y., Low-temperature synthesis/densification and properties of Si_2N_2O prepared with Li_2O additive. *J. Eur. Ceram. Soc.*, 2007, **27**, 4767–4772.
63. Šajgalík, P., Dusza, J., Lenčéš, Z., Hnatko, M., Galusek, D. and Ghillányová, K., Bulk ceramic nanostructures. In *Ceramics Science and Technology*, *vol. 1*, ed. I-Wei Chen. Wiley-VCH Verlag GmbH, Weinheim, 2008, pp. 347–373.
64. de Arellano-López, A. R., Varela-Feria, F. M., Martínez-Fernandez, J. and Singh, M., Compressive creep of silicon nitride with different secondary phase compositions. *Mater. Sci. Eng.*, 2002, **A332**, 295–300.